Exploring the Energy Landscape of Antibody−Antigen Complexes: Protein Dynamics, Flexibility, and Molecular Recognition

Megan C. Thielges,[‡] Jörg Zimmermann,[‡] Wayne Yu,[‡] Masayuki Oda,[§] and Floyd E. Romesberg*[,‡]

Department of Chemistry, The Scripps Research Institute, 10550 North Torrey Pines Road, La Jolla, California 92037, and Graduate School of Agriculture, Kyoto Prefectural University, 1-5 Hangi-cho, Shimogamo, Sakyo-ku, Kyoto 606-8522, Japan

Received March 4, 2008; Revised Manuscript Received May 14, 2008

ABSTRACT: The production of antibodies that selectively bind virtually any foreign compound is the hallmark of the immune system. While much is understood about how sequence diversity contributes to this remarkable feat of molecular recognition, little is known about how sequence diversity impacts antibody dynamics, which is also expected to contribute to molecular recognition. Toward this goal, we examined a panel of antibodies elicited to the chromophoric antigen fluorescein. On the basis of isothermal titration calorimetry, we selected six antibodies that bind fluorescein with diverse binding entropies, suggestive of varying contributions of dynamics to molecular recognition. Sequencing revealed that two pairs of antibodies employ homologous heavy chains that were derived from common germline genes, while the other two heavy chains and all six of the light chains were derived from different germline genes and are not homologous. Interestingly, more than half of all the somatic mutations acquired during affinity maturation among the six antibodies are located in positions unlikely to contact fluorescein directly. To quantify and compare the dynamics of the antibody−fluorescein complexes, three-pulse photon echo peak shift and transient grating spectroscopy were employed. All of the antibodies exhibited motions on three distinct time scales, ultrafast motions on the <100 fs time scale, diffusive motions on the picosecond time scale, and motions that occur on time scales longer than nanoseconds and thus appear static. However, the exact frequency of the picosecond time scale motion and the relative contribution of the different motions vary significantly among the antibody−chromophore complexes, revealing a high level of dynamic diversity. Using a hierarchical model, we relate the data to features of the antibodies' energy landscapes as well as their flexibility in terms of elasticity and plasticity. In all, the data provide a consistent picture of antibody flexibility, which interestingly appears to be correlated with binding entropy as well as with germline gene use and the mutations introduced during affinity maturation. The data also provide a gauge of the dynamic diversity of the antibody repertoire and suggest that this diversity might contribute to molecular recognition by facilitating the recognition of the broadest range of foreign molecules.

The immune system rapidly generates high affinity antibodies (Ab[1]) that are specific for virtually any foreign target (or antigen) via combinatorial recombination of a diverged set of gene fragments (germline genes), junctional diversity generated during recombination, and somatic mutations introduced during affinity maturation after the functional Ab has encountered its antigen (*1–6*). The role of sequence variation in generating a diverse repertoire of receptors has been studied intensively and has made Ab a paradigm for understanding molecular recognition (*4, 5*). However, proteins are inherently dynamic, and there is a growing appreciation that dynamics may contribute to biological function (*7–13*). For example, protein dynamics differentiates the limiting models of molecular recognition: lock-and-key and induced fit or conformational selection. Lock-and-key receptors require relative rigidity and conformational homogeneity, while induced fit or conformational selection receptors require relative flexibility and conformational heterogeneity. Differences in protein dynamics are also implicit in the classical models of immune function: the clonal selection theory (*14, 15*) evokes relatively rigid and conformationally homogeneous Ab, while the instructive hypothesis (*16, 17*) evokes more flexible and conformationally heterogeneous receptors. In addition, while many Ab are known to be exquisitely specific, the number of potential antigens far exceeds the number of available Ab, which suggests that at least some Ab must be polyspecific and hence sufficiently dynamic and plastic to accommodate different antigens (*18–21*).

Most efforts to understand the structural and/or functional diversity of Ab−antigen complexes have focused on their characterization using X-ray crystallography (*22–27*). Ab are typically found to accommodate different small molecule antigens by burying them within a combining site formed by six loops of hypervariable sequence (called complementarity-determining regions, or CDRs), three from the Ab heavy chain, V_H, and three from the Ab light chain, V_L. The

* To whom correspondence should be addressed. Tel: (858) 784-7290. Fax: (858) 784 7472. E-mail: floyd@scripps.edu.

[‡] The Scripps Research Institute.

[§] Kyoto Prefectural University.

[1] Abbreviations: Fl, fluorescein; Ab, antibodies; CDR, complementarity-determining regions; V_L, light-chain variable region; V_H, heavy-chain variable region; 3PEPS, three-pulse photon echo peak shift; UTR, untranslated region; fs, femtosecond; ps, picosecond.

10.1021/bi800374q CCC: $40.75
Published on Web 06/13/2008

sequence diversity of the CDRs allows for a high level of shape and electrostatic complementarity between the combining site and the different antigens. Structural studies have also shown that at least some Ab are able to accommodate multiple, different antigens within their combining sites (*27*). While this is consistent with Ab flexibility, these studies do not provide an actual measure of protein dynamics. To address the potential contribution of protein dynamics to Ab function, a more direct characterization is required.

The ability to characterize the dynamics of a chromophore and its environment has been revolutionized by ultrafast nonlinear spectroscopies, such as three-pulse photon echo peak shift (3PEPS) spectroscopy (*28–30*). These experiments rely on the application of a force to the chromophore's environment that originates from an excitation-induced change in the chromophore's dipole moment. The time scale and energy of the environment's response to this force are characterized by following the coherence decay in the ensemble of excited chromophores, which yields the energy gap autocorrelation function, $M(t)$, which is conveniently represented in the frequency domain with the corresponding spectral density, $\rho(\omega)$ (*31*). Additionally, dynamics that appear static on the time scale of the 3PEPS experiment are manifest as a nonzero asymptote of the peak shift, thus allowing the detection and quantification of conformational heterogeneity (*30, 31*).

To study Ab dynamics via 3PEPS spectroscopy, we have employed murine Ab evolved to bind different chromophoric antigens, including fluorescein (Fl) (*32–34*). The Ab are expected to bind a chromophore as they would any other small molecule antigen, deep in a hydrophobic binding pocket, well packed by CDR loops, and sequestered from solvent. This has been confirmed by structural studies for the anti-Fl Ab 4-4-20 (*35*). Thus, Fl is not expected to probe solvent dynamics, but rather to probe biologically relevant protein motions that are generally representative of any Ab−antigen complex (*36*). Previously, we used 3PEPS spectroscopy to characterize three different anti-Fl Ab (*32*). Despite the absence of any significant sequence homology, we observed similar motions in the three Ab that differed mainly in amplitude, and similar levels of static inhomogeneity. However, it remains unclear whether such limited dynamic diversity is representative of all mature Ab.

Here, we report the thermodynamic, amino acid sequence, and protein dynamics analysis of six anti-Fl Ab, including two whose dynamics and sequences have been reported previously, 4-4-20 and 34F10, and four that have not been characterized previously, 56G2, 18B7, 4D4, and 1F10. The Ab were chosen because they display a broad range of binding entropies, which we reasoned might result, at least in part, from differing levels of flexibility and/or conformational heterogeneity in the Ab-Fl complexes. Sequence analysis reveals that while some homology exists between the Ab, they are mostly diverse, and the 3PEPS and transient grating (TG) spectroscopy reveal that this sequence diversity is manifest as significant dynamic diversity. Interestingly, at least approximate correlations are observed between the dynamics of the Ab-Fl complexes and the thermodynamics, germline gene use, and extent of affinity maturation. The data suggest that the immune system may employ Ab with diverse dynamics and that it may even tailor dynamics during affinity maturation in order to most efficiently recognize the broadest range of foreign antigens.

EXPERIMENTAL PROCEDURES

Generation and Sequencing of Anti-Fl Ab. Monoclonal hybridoma cell lines were produced by standard techniques after injecting BALB/c (in the case of 18B7 and 4D4) or 129/Sv (in case of Ab 34F10, 56G2, and 1F10) mice with bovine serum albumin-Fl conjugate. Monoclonal Ab 4-4-20 ascites was kindly provided by Professor Edward Voss (University of Illinois). Anti-Fl monoclonal IgG Ab were purified from ascite supernatants by standard methods. The DNA sequences of the mature Ab 4-4-20 and 34F10 have been reported previously (*32*). For the remaining four Ab, V_H and V_L gene sequences were determined using cDNA prepared from mRNA isolated from fresh hybridoma cells. Approximately 10^6 hybridoma cells were washed in cold phosphate buffered saline (PBS) and subjected to alkaline lysis, after which oligonucleotide $(dT)_{18}$ was annealed to the cellular mRNA. cDNA was then synthesized using reverse transcriptase (Ambion). PCR amplification of the Ab genes from cDNA was accomplished using a primer set specific for cloning mouse immunoglobulin regions (*37, 38*) and each product was sequenced using standard techniques.

The germline V_H and V_L sequences of Ab 4-4-20 were reported previously (*33*). For the remaining five Ab, candidate germline sequences were identified by comparing the sequences obtained from the cDNA to published V_H and V_L sequences (Supporting Information). Briefly, in the case of the 34F10, 56G2, and 1F10 V_H chains, sequence searches were performed with the 129/Sv V_H sequences (*39*) (http://www.imgt.cines.fr; http://www.ncbi.nlm.nih.gov). However, in the case of the 34F10, 56G2, and 1F10 V_L chains, and the 18B7 and 4D4 V_H and V_L chains, all available genomic sequences were employed; as in these cases, the genome sequence data is incomplete. On the basis of the identified germline candidates, primers were designed to amplify the 5′ untranslated region (UTR) of each gene from both the hybridoma and either 129/Sv or BALB/c genomic DNA (obtained from The Jackson Laboratory). Using this approach, we identified the germline V_H and V_L genes with the most homologous 5′ UTR regions (see also Table S1 in Supporting Information).

Isothermal Titration Calorimetry. Isothermal titration calorimetric experiments were performed using a MicroCal MCS calorimeter and analyzed with VP-ITC software (MicroCal Inc., Northampton, MA). The heat generated or absorbed was measured during the titration of 150 μM fluorescein in PBS into 8 μM IgG in PBS. Solutions were thoroughly degassed prior to use. Each titration consisted of a single preliminary injection, followed by 20 successive 10 s injections every 240 s. The heat of dilution of the titrant was accounted for by performing the titration into a blank PBS buffer solution. The $T\Delta S^\circ$ values were determined from the $\Delta H^\circ - \Delta G^\circ$ values. The ΔC_p° values were calculated from a linear fit of ΔH° values determined at different temperatures ranging from 293 to 308 K (Table S2 in Supporting Information). Standard deviations for the thermodynamic parameters were determined from the standard error of the least-squares regressions.

To better assess the entropic changes associated with

protein dynamics, we deconvoluted the total entropy change into the entropy change associated with solvent release, $\Delta S°_{solv}$, the entropy change due to loss of translational and rotational degrees of freedom, $\Delta S°_{rt}$, and the entropy change from changes of internal motions of protein and ligand, $\Delta S°_{conf}$ (*40*). For the association of two molecules, $\Delta S°_{rt}$ is estimated to contribute -8 cal K^{-1} mol^{-1} by statistical mechanical arguments (*41, 42*). $\Delta S°_{solv}$ is typically assumed to be dominated by the hydrophobic contribution due to the burial of apolar surface area, $\Delta C_p° \ln(T/T_S*)$, where T_S* is 385 K and $\Delta C_p°$ is the change in heat capacity upon binding (*41*). Thus, the conformational entropy of binding may be estimated as,

$$\Delta S° = \Delta S° + 8 \text{ cal } K^{-1}mol^{-1} - \Delta C_p° \ln(T/385 \text{ K}) \quad (1)$$

3PEPS and Transient Grating Experiments. Samples contained 100 μM Ab and 80 μM Fl in PBS. The Ab were washed extensively with PBS by repeated dilution and microfiltration (10,000 MWCO, Amicon) to remove unbound fluorescein, the absence of which was confirmed by UV/vis spectroscopy. Absorption spectra of the Ab-Fl complexes were acquired in a 1 cm quartz cuvette using an HP8453a spectrophotometer. The experimental setup for 3PEPS and TG has been described previously (*43*). Briefly, a Ti:Sa regenerative amplifier system (Spectra Physics Spitfire, 5 kHz, 200 mJ pulses at 800 nm) was used to pump a home-built NIR-OPA. The 1.3−1.6 μm output of the NIR-OPA was mixed with the pump beam (800 nm) in a type I BBO crystal to generate 490−510 nm pulses (∼45 − 50 fs, 50 nJ). The beam was compressed by a pair of fused silica prisms and split into three roughly equal portions. One beam was set to travel a fixed distance, while the other two were allowed to travel independently variable distances by the use of delay stages (Kensington Laboratories, PM6000). The pulse duration was measured via autocorrelation to be ∼50 fs. The three beams were arranged in an equilateral triangle of ∼7 mm per side and focused on the sample with a 200 mm focal length plano-convex fused silica lens. A spinning cell with a path length of 200 μm was used and maintained at 22 °C ± 1 °C. Typical pulse energies at the sample were 2−5 nJ per pulse. The transient grating and photon echo signals in the two phase matching directions $k_1 - k_2 + k_3$ and $-k_1 + k_2 + k_3$ were spatially filtered and detected with large area avalanche photodiodes (Advanced Photonics). A phase-locked chopper (New Focus), synchronized with the Q-switch of the regenerative amplifier, was used to chop the fixed delay beam. Two lock-in amplifiers (Stanford SR830) referenced to the chopper were used to sample the output of the detectors.

For the TG measurements, the delay between the first and second pulse was set to zero, and the delay of the third pulse was scanned from −5 ps to 50−300 ps. Ten scans were averaged for each TG experiment. The parameters from 3 to 4 TG experiments were averaged, and standard deviations were calculated. For the 3PEPS experiments, the coherence period, τ, the delay between the first and second pulses, was scanned from −150 to 150 fs for a fixed value for the population period, T, the delay between the second and third pulses. The average shift from zero of the temporal signal maximum in τ for the two phase-matching directions is referred to as the peak shift for a given population time, T. Five to 10 scans at a given population time were averaged for a total of 20−50 population times. To ensure reliable comparison of the Ab, at least four independent experiments were performed, independently analyzed, and averages and standard deviations calculated. In addition, the terminal peak shift (100 ps population time) of the previously characterized Ab 4-4-20 (*32–34*) was measured before each day of experiments to ensure reproducibility.

Spectroscopic Data Analysis. Transient grating data were fit to mono- or double-exponential decays (Origin 6.0, Microcal). In order to assess the number of time scales present in the 3PEPS decays, the data were fit to a sum of exponential decays. From this initial analysis, we found that three time scales (two exponential decay terms and an offset) were required to fit the decays, and that inclusion of additional terms was not statistically justified (Supporting Information). The experimental 3PEPS decays were then fit using a model spectral density function according to Mukamel's response function formalism (*31*), similar to procedures described previously (*34*). However, while previously the parameters were adjusted manually, in this study both the steady state absorption spectra and the 3PEPS decay were simultaneously fit by least-squares error analysis, as described below. The total spectral density, $\rho(\omega)$, was calculated from the sum of the vibrations of the chromophore, $\rho_{Fl}(\omega)$, and the vibrations of the protein, $\rho_{Ab}(\omega)$. Intramolecular vibrational frequencies and excitation-induced displacements of Fl were obtained from quantum chemical calculations and validated by experimentally determined Raman frequencies, as described in ref *32*. $\rho_{Ab}(\omega)$ was modeled as the sum of two components, an underdamped Brownian oscillator term (which we refer to as the Brownian oscillator term) for the fastest motions and an overdamped Brownian oscillator term (which we refer to as the Kubo term) for slower motions: $\rho_{Ab}(\omega) = \rho_{BO}(\omega) + \rho_K(\omega)$. Specifically, the underdamped Brownian oscillator term

$$\rho_{BO}(\omega) = \frac{2\lambda_{BO}}{\pi\omega} \frac{\omega_{BO}^2 \Gamma_{BO}}{(\omega_{BO}^2 + \omega^2)^2 + \Gamma_{BO}^2 \omega^2} \quad (2)$$

was used to represent the inertial subpicosecond protein dynamics, where λ_{BO} is the reorganization energy, ω_{BO} is the frequency, and Γ_{BO} is the damping constant of the Brownian oscillator, and the Kubo term

$$\rho_\kappa(\omega) = \frac{\lambda_\kappa}{\pi\omega} \frac{\tau_\kappa}{1 + \omega^2 \tau_\kappa^2} \quad (3)$$

was used to represent the picosecond dynamics, where λ_K and τ_K are the reorganization energy and time constant, respectively. Signals for the 3PEPS experiment and the steady-state absorption spectra were calculated from the line-broadening function $g(t)$ by using standard procedures (*28, 29, 31*). $g(t)$ was calculated from $\rho(\omega)$ using the following expression.

$$g(t) = i\int_0^\infty d\omega \rho(\omega) \sin(\omega t) + \int_0^\infty d\omega \rho(\omega) \coth\left(\frac{\hbar\omega}{2k_B T}\right)[1 - \cos(\omega t)] + \frac{(\Delta_{inh} t)^2}{2} \quad (4)$$

The parameters in $\rho_{Ab}(\omega)$ and the amount of static inhomogeneity, Δ_{inh}, in $g(t)$ were varied using a least-squares fit algorithm (Matlab 6.0) to obtain the best fit of both the experimental 3PEPS data and the steady state absorption

Table 1: Thermodynamic Data

Ab	$\Delta G^{\circ a}$	$\Delta H^{\circ a}$	$T\Delta S^{\circ a}$	$\Delta C_P^{\circ b}$	$T\Delta S^{\circ}_{conf}{}^{a}$
34F10	−11.7 ± 0.15	−19.7 ± 0.09	−8.0 ± 0.17	−0.20 ± 0.010	−20.9 ± 3.0
8D11	−10.3 ± 0.01	−14.8 ± 0.25	−4.5 ± 0.25	−0.15 ± 0.001	−13.6 ± 0.39
56G2	−10.7 ± 0.14	−14.3 ± 0.11	−3.6 ± 0.18	−0.18 ± 0.004	−15.0 ± 0.18
33C5	−11.1 ± 0.17	−13.9 ± 0.14	−2.8 ± 0.22	−0.16 ± 0.009	−12.6 ± 0.22
40G4	−8.8 ± 0.11	−10.8 ± 0.23	−2.0 ± 0.25	−0.15 ± 0.014	−11.1 ± 4.2
4-4-20	−11.3 ± 0.12	−12.5 ± 0.08	−1.2 ± 0.14	−0.23 ± 0.008	−16.4 ± 2.4
4D4	−11.1 ± 0.26	−11.6 ± 0.14	−0.5 ± 0.30	−0.18 ± 0.004	−11.9 ± 1.2
1F10	−10.9 ± 0.19	−7.6 ± 0.07	3.3 ± 0.20	−0.18 ± 0.021	−8.1 ± 6.3
18B7	−10.9 ± 0.21	−3.6 ± 0.04	7.3 ± 0.21	−0.24 ± 0.005	−8.6 ± 1.5

[a] kcal/mol, $T = 298$ K. [b] kcal/mol/K.

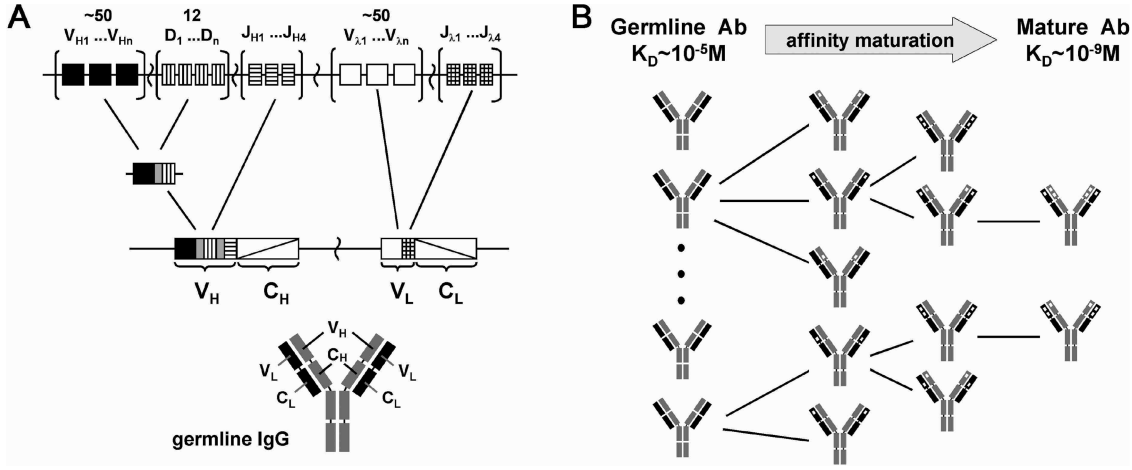

FIGURE 1: (A) Genetic origins of Ab sequence diversity. V_L, C_L, V_H, and C_H correspond to variable and constant regions of the light and heavy chains, respectively. (B) Ab affinity maturation. Individual clones of the germline repertoire are selected by antigen and acquire mutations, represented as small open circles, during proliferation.

spectra using a custom suite of programs (Dr. Delmar Larsen, University of California, Davis). Because the amplitude, λ_{BO}, frequency, ω_{BO}, and damping constant, Γ_{BO}, of the Brownian oscillator term could not be fit unambiguously, we fixed the values of ω_{BO} and Γ_{BO} to those previously determined for Ab 4-4-20 (*34*). Simulation of the data with different values for these fixed terms resulted in only small variations in the remaining terms.

RESULTS

Thermodynamics of Antigen Recognition and the Selection of Six Potentially Diverse Ab. To gauge the thermodynamic diversity of an immune response, nine anti-Fl Ab were examined by isothermal titration calorimetry to determine the changes in free energy (ΔG°), enthalpy (ΔH°), entropy (ΔS°), and heat capacity (ΔC_p°) associated with Fl binding (Table 1). Similar ΔG° values were observed, ranging only between −8.8 and −11.6 kcal/mol, with an average of −10.8 ± 0.8 kcal/mol. The similar ΔG° values likely reflect the limits in selection pressure during an immune response (i.e., only a certain affinity is required to clear an infection). Unlike ΔG°, large variations are observed for ΔH° and ΔS° (Figure 2). This effect, referred to as enthalpy−entropy compensation, has been observed previously with Ab (*44*) as well as with other biological systems (*45*) and suggests that the necessary level of molecular recognition may be achieved with different combinations of enthalpy and entropy driven processes.

For Ab 34F10, Fl recognition is driven by ΔH°, and binding occurs despite a large and unfavorable ΔS°. For Ab

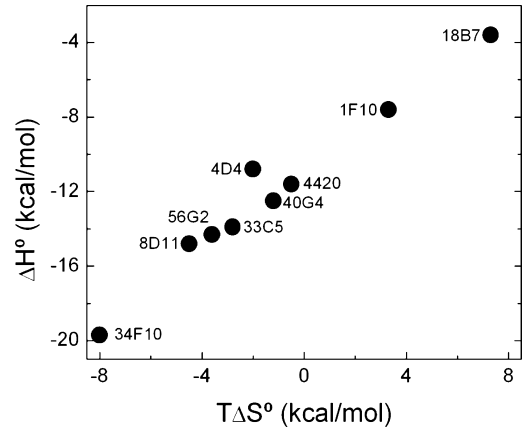

FIGURE 2: Correlation between binding enthalpy and entropy of anti-Fl Ab ($T = 298$ K).

8D11, 56G2, 33C5, 40G4, 4-4-20, and 4D4, we observed decreasingly favorable ΔH° values accompanied by increasingly favorable ΔS° values. For Ab 1F10 and 18B7, the changes in entropy are positive, and for 18B7, $T\Delta S^{\circ}$ actually contributes more to binding than ΔH°. The Ab all showed similar large and negative ΔC_p° values, suggesting that in each case Fl is sequestered from solvent (*46*), as is also implied by the binding-induced red shifts in the absorption maxima of all Ab (see below) as well as the structure of the 4-4-20-Fl complex (*35*). The ΔC_p° values also allow for the estimation of the changes in conformational entropy of the protein and ligand, ΔS°_{conf}, which at room temperature vary between −8.1 kcal/mol for Ab 1F10 and −20.9 kcal/mol for Ab 34F10 (Table 1). The different $T\Delta S^{\circ}_{conf}$ values may reflect different levels of protein dynamics in the free

A

```
4420L   DVVMTQTPLSLPVSLGDQASISCRSSQSLVHSNGNTYLRWYLQKPGQSPKVLIYKVSNRFSGVPDRFSGSGSGTDFTLKISRVEAEDLGVYFCSQSTHVPWTFGGGTKL
        ------------------------------------H----------L-------------------------------------------------------
34f10L  DIQMNQSPSSLSASLGDTITITCHASQNINIWLNWYQQKPGNVPNLLIYKASNLHTGVPSRFSGSGSGTGFTLTISSLQPEDIATYYCQQGQSYPLTFGAGTKLEIR
        -----------------------------V--S--------I-K-----------------------------------------------------
56G2L   DIVMTQSHKFMSTSVGDRVSITCKASQDVSTTVAWYQQKPGQSPKLLIYSASYRYTGVPDRFTGSGSGTDFTFTISSVQAEDIAVYYCQQHYSTPPTFGGGTKLEIK
        ----------------------------------A-----------------------------------------------------------------
18B7L   DVVMTQTPLTLSVTIGQPASISCKSSQTLLDSDGKTYLNWLLQRPGQSPKRLIYLVSRLDSGVPDRFTGSGSGTDFTLKISRVEAEDLGVYYCWQGTHFPRTFGGGTKLEIK
        -------------------------S-----------------------K-----------------------------------------------------
4D4L    QAVVTQESALTTSPGETVTLTCRSSTGAVTTSNYANWVQEKPDHLFTGLIGGTNNRAPGVPARFSGSLIGDKAALTITGAQTEDEAIYFCALWYSNHLVFGGGTKLTVL
        ------------------------------------------------------------------------------------------------------
1F10L   ENVLTQSPTIMSASPGEKVTMTCRASSSVSSNYLHWYQQKSGASPKLWIYSTSNLASGVPARFSGSGSGTSYSLSISSVEAEDAATYYCQQYSGYPFTFGGGTKLEIK
        --------A----------------------S-------------------------------------------T--------------------
```

B

```
4420H   EVKLDETGGGLVQPGRPMKLSCVASGFTFSDYWMNWVRQSPEKGLEWVAQIRNKPYNYETYYSDSVKGRFTISRDDSKSSVYLQMNNLRVEDMGIYYCTGSYYGMDYWGQGYSVTVSS
        ---------------S------------TNS----FC-----------KS-----------------------------------A--T-----------------------
34F10H  EVKLVESGGGLVQPGNSLRLSCATSGFTFTDYFMTWVRQPPGKALEWLGFNRNRANGFTTEYNPSVKGRFAISRDNSQNILYLQMNDLRPEDSATYYCARDPPFLRVFDYWGQGTTLTVSS
        ---------------G----------------Y-S---------------I--K---Y----SA------T-------S-------T--A----------
56G2H   EVKLVESGGGLVQPGDSLRLSCATSGFTFIDYYMYWVRQPPGKTLEWLGFIRKRAYGYTTEYSASVKGRFTISRDNSQNILYLQMTTLRPEDSATYYCASGGYGNYVGFSYWGQGTLVTVST
        ---------------G------------T----S--------A--------NK-N---------------------S------N------------R
18B7H   QIQLVQSGPELKKPGETVKISCKASGFTFTSYGLSWVKQAPGEGLKWMGWINTYSGVPTYVDDFKGRIAFSLETSASTAYLQINNLNNEDAATYFCARLTTVMPWYWGQGTTLTVSS
        -------------------------Y---T--M--------K----------------A------F-----------------K---T-------
4D4H    QIQLIQSGPELKKPGETVKISCKTSGYTYTTYGMSWVKQAPGKGLKWMGWINTYSGVPTYADDFKGRFDFSLETSASTVYLQINNLKNEDMATYFCARRLRRDWYFDAWGTGTTVTVSS
        ----V------------------A----F---------------------------------------A---------A----------T-------
1F10H   QVQLKESGPGLVAPSQSLSITCAVSGFSLTTYGVHWVRQPPGKGLEWLGVIWAGGSTYYNSALMSRLSITKDNSKSHVFLKMNSLQTDDTAIYYCARRYHGGIYYAMDYWGQGSSVTVSS
        ---------------------T-------S-------------------------N----------S------Q--------------M-----
```

FIGURE 3: Ab sequences. Sequences of mature Ab with germline antecedent shown below for (A) each light chain and (B) each heavy chain. Identity is indicated by a dash, and the CDRs are underscored.

Ab and/or in the Ab-Fl complexes. Thus, six of the Ab, whose $T\Delta S°$ terms range from −8.0 kcal/mol to +7.3 kcal/mol, were selected for further characterization: 34F10, 56G2, 4-4-20, 4D4, 1F10, and 18B7.

Sequences of the Mature and Germline Progenitor Ab. The nucleotide sequences of the mature Ab V_H and V_L genes were determined from gene fragments amplified by PCR with Ab specific primers (*37, 38*) and template cDNA obtained from corresponding hybridoma cells. The identification of the progenitor germline genes was based on the homology of the 5′ UTRs of the rearranged Ab genes and genomic germline genes (see Experimental Procedures and Supporting Information). The sequences of the mature Ab and their germline antecedents are shown in Figure 3. Each Ab evolved from a different V_L germline gene, and no significant sequence homology is observed for any of the V_L CDRs. However, the V_H chains of 34F10 and 56G2 both descended from the IGHV7-3 germline gene (*39*), and those of 18B7 and 4D4 both descended from the IGHV9-3 germline gene (*39*). Thus, these V_H sequences have significant homology with each other but not with the other V_H sequences. The somatic mutations introduced during affinity maturation were identified by comparing the mature and germline sequences (Figure 3). As reported previously, affinity maturation of Ab 4-4-20 introduced 2 V_L mutations and 10 V_H mutations. For 34F10, 56G2, 18B7, 1F10, and 4D4, affinity maturation appears to have introduced 4, 1, 2, 3, and 0 V_L mutations and 12, 10, 8, 6, and 6 V_H mutations, respectively. From this data, it is apparent that 34F10 is the most highly somatically mutated (with 16 mutations introduced), followed by 4-4-20 (12 mutations), 56G2 (11 mutations), 18B7 (10 mutations), 1F10 (9 mutations), and 4D4 (6 mutations). Thus, as suggested by the binding data, the Ab are diverse in terms of both sequence and extent of affinity maturation.

Dynamics of Ab−Antigen Complexes. The absorption spectra of free Fl and Fl bound to each of the six anti-Fl Ab are shown in Figure 4A. The spectra are similar for the six Ab, with absorption maxima that range from 499 to 506 nm, significantly red-shifted from the absorption maximum of 491 nm for free Fl in aqueous buffer at pH 7. TG experiments were used to determine the excited-state lifetime of Fl when

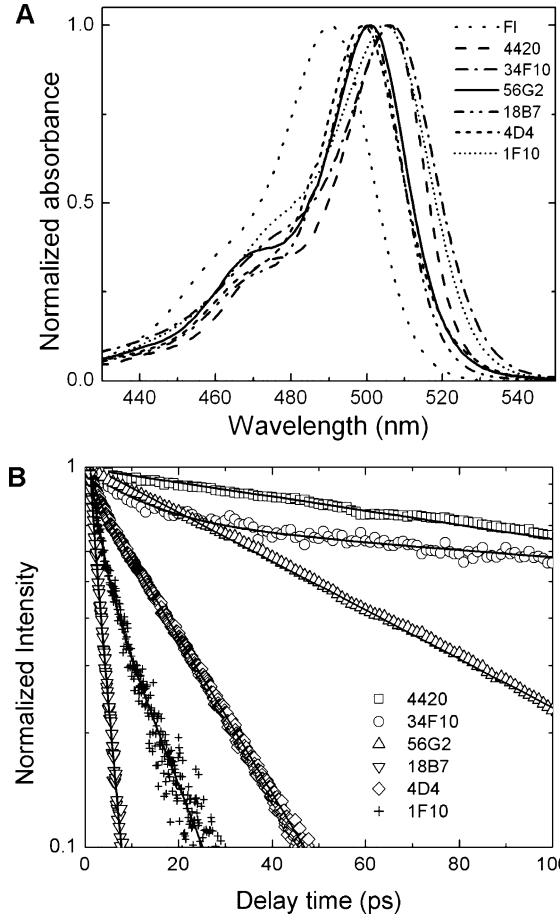

FIGURE 4: (A) Normalized absorption spectra of Fl in buffer or bound to the different Ab. (B) TG decays for Fl bound to the different Ab. Lines are best fits to the data (Table 2).

bound to the different Ab (Figure 4B and Table 2). A fast decay component was required to fit several of the TG decays to account for coherent dynamics. The population dynamics could be fit with a single exponential decay for all Ab, with excited-state lifetimes ($2\tau_{TG}$) between 8 and 460 ps, except 34F10, which was fit to a double-exponential decay with life times of 32 ps and 1.1 ns. The shorter lifetimes in 4D4,

Table 2: Transient Grating Fit Parameters

Ab	a_1	τ_1 (ps)	a_2	τ_2 (ps)
4-4-20	1	230 ± 30		
34f10	0.7 ± 0.02	530 ± 100	0.3 ± 0.02	16 ± 3
56G2	1	65 ± 12		
18B7	0.8 ± 0.1	4 ± 1	0.2 ± 0.1	0.7 ± 0.3
4D4	0.7 ± 0.2	17 ± 5	0.3 ± 0.2	1.4 ± 0.3
1F10	0.6 ± 0.1	12 ± 1	0.4 ± 0.1	1.6 ± 0.1

18B7, and 1F10 account for the loss in signal observed at long population times in the 3PEPS experiments (see below). The differences in lifetimes likely reflect sequence differences, for example, the presence or absence of specific Trp residues that pack with and quench the chromophore.

3PEPS experiments were used to measure Ab dynamics. The results obtained for 4-4-20 and 34F10 agree with those reported previously (*32*). 3PEPS decays were measured up to 150 ps population time, except for Ab 4D4, 18B7, and 1F10, where the lifetime of the bound Fl limited the accessible experimental time window. Nevertheless, in each case the Fl lifetime was much longer than the electronic coherence time (~30 fs); thus, while the relatively short lifetimes of Fl bound to 4D4, 18B7, and 1F10 decrease the echo signal intensity for long population times, they are not expected to affect the peak shift value (*47, 48*). $M(t)$ and $\rho_{Ab}(\omega)$ were calculated from the data as described in Experimental Procedures.

Both similarities and significant differences are observed among the six Ab-Fl complexes (Figure 5 and Table 3). With each of the six Ab, motions on three distinct time scales were observed: an ultrafast (sub-100 fs) time scale motion that likely represents barrierless side chain motions; an intermediate (picosecond) time scale motion that likely reflects activated backbone and CDR loop fluctuations; and a longer (nanosecond or longer) time scale motion that appears static in the 3PEPS experiment and likely reflects conformational diversity of the Ab combining site (*36, 49*). Interestingly, the time scale of the intermediate motion varies among the Ab. In 4-4-20, the intermediate time scale motion is relatively low frequency (τ_K = 5.2 ps), while it is higher frequency in 34F10 and 56G2 (τ_K = 2.9 and 2.3, respectively) and the highest with 18B7, 4D4, and 1F10 (τ_K = 0.6 − 0.8 ps).

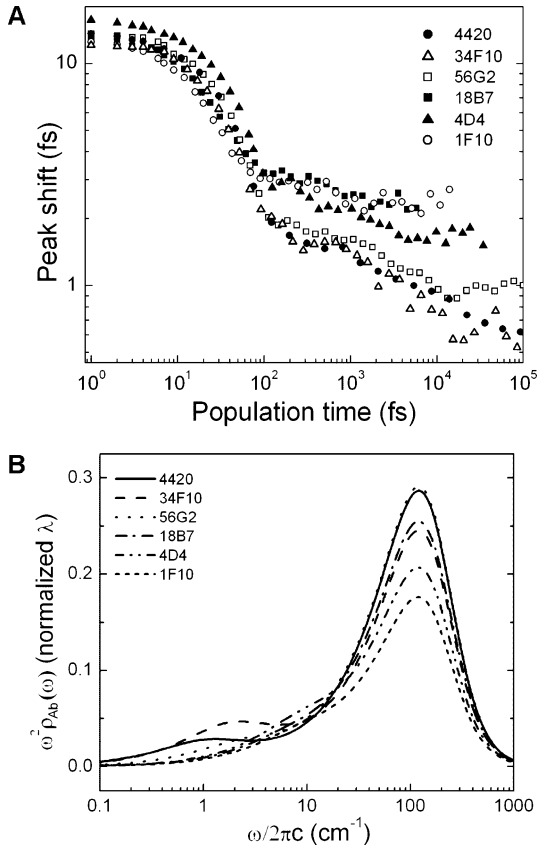

FIGURE 5: (A) 3PEPS decays for each Ab-Fl complex. (B) Spectral densities normalized by the total reorganization energy.

Table 3: 3PEPS $\rho_{Ab}(\omega)$ Parameters

Ab	λ_{BO} (cm^{-1})	ω_{BO} (cm^{-1})[a]	Γ_{BO} (cm^{-1})[a]	λ_K (cm^{-1})	τ_K (ps)	Δ_{inh} (cm^{-1})
4-4-20	187 ± 39	200	380	42 ± 7	5.2 ± 2.8	136 ± 62
34F10	204 ± 62	200	380	87 ± 12	2.9 ± 1.4	160 ± 26
56G2	221 ± 31	200	380	39 ± 8	2.3 ± 0.8	157 ± 21
18B7	173 ± 32	200	380	35 ± 9	0.8 ± 0.3	181 ± 28
4D4	158 ± 62	200	380	70 ± 34	0.6 ± 0.2	208 ± 37
1F10	200 ± 39	200	380	76 ± 26	0.6 ± 0.3	301 ± 28

[a] Fixed during fit.

Table 4: Normalized Reorganization Energies

Ab	λ_{BO}	λ_K	λ_{inh}[a]
4-4-20	0.68	0.15	0.16
34F10	0.58	0.25	0.17
56G2	0.69	0.12	0.18
18B7	0.60	0.12	0.27
4D4	0.48	0.21	0.31
1F10	0.41	0.15	0.44

[a] $\lambda_{in} = \Delta_{in}^2/2kT$.

While the differences in amplitude of the inertial response for the most part are not statistically significant, the amplitudes of the intermediate and long time scale motions differ significantly, and thus, the relative contribution of each time scale of motion to the total reorganization energy in each Ab-Fl complex is different (Table 4). As a percentage of total reorganization energy, Ab 56G2 and 4-4-20 shows the greatest amount of fast motion (~69% of the reorganization energy), followed by 18B7 and 34F10 (58−60%), with less in 4D4 (48%), and the least in 1F10 (41%). The extent of the reorganization energy accommodated by the picosecond time scale motion was 21−25% for Ab 34F10 and 4D4, and 12−15% for Ab 4-4-20, 56G2, 18B7, and 1F10. The relative amplitude of the slowest motions varied between less than 20% (4-4-20, 34F10, and 56G2) to 27% (18B7), 31% (4D4), and 44% (1F10).

DISCUSSION

Molecular recognition is central to the biological functions of proteins, and the immune system has served as a paradigm for its study. The last century saw the emergence of two competing models of Ab−antigen recognition, and these two models make rather different predictions about Ab dynamics. The clonal selection theory of Jerne (*14*) and Burnet (*15*) proposes that the sequence of an Ab programs it to recognize a specific antigen and thus evokes rather rigid and conformationally homogeneous Ab. The instructive hypothesis, first proposed by Breinl and Haurowitz (*16*) and later developed by Pauling (*17*), assumes that Ab-combining sites are plastic and adopt the appropriate conformation for binding a given

antigen only in the presence of that antigen and thus evoke rather flexible and conformationally heterogeneous Ab. With the discovery that antigens select specific Ab from a repertoire of already functional receptors, the clonal selection theory, with its rigid and conformationally homogeneous Ab, received widespread acceptance. However, because the potential number of foreign molecules recognizable by the immune system far exceeds the potential number of different Ab, which is limited by available B-cells (*18*), some Ab must be polyspecific, suggesting the presence of at least some plasticity. The differences in Ab flexibility implied by these different models reflect the important role that dynamics plays in molecular recognition and motivates its rigorous analysis.

Thermodynamic, Sequence, and Dynamic Diversity. In an initial thermodynamic characterization of a panel of nine anti-Fl Ab, we found that they all bind Fl with similar affinity but with very different $\Delta H°$ and $T\Delta S°$ values. Because Ab that bind Fl with different changes in entropy are likely to be dynamically diverse, six Ab were selected for further study on the basis of their $T\Delta S°$ values, which ranged from −8.0 to +7.3 kcal/mol (see Table 1). At the two extremes are Ab 34F10, whose recognition of Fl is driven purely by enthalpic changes, and Ab 18B7, whose Fl recognition is predominantly entropically driven.

To initiate an immune response, a member of the repertoire of naïve germline Ab must first be selected on the basis of affinity for the antigen. It is thus perhaps not surprising that two sets of Ab V_H chains evolved from the same progenitor genes: the V_H chains of 34F10 and 56G2 from the germline gene IGHV7-3 and the V_H chains of 4D4 and 18B7 from the germline gene IGHV9-3. This suggests that both IGHV7-3 and IGHV9-3 encode V_H chains that efficiently recognize Fl. However, there is little homology between these two germline genes, between these two genes and the genes that encode the 4-4-20 or 1F10 V_H chains, or between any of the V_L chains, which appear to have each descended from a different germline gene. From these sequence data, it is clear that a wide variety of combining sites can provide suitable starting points for the evolution of high affinity anti-Fl Ab. In addition, it is interesting to note that more than half of the somatic mutations occur outside of CDR loops. These mutations are unlikely to optimize direct interactions with Fl, but rather must have been selected on the basis of secondary interactions, possibly tailoring protein dynamics (*34*).

The large red shift in the absorption of Fl upon binding suggests that Fl is bound in a hydrophobic environment and is sequestered from solvent in each Ab-Fl complex. In general, Ab always bind small molecule antigens such as Fl in a well packed, deep, hydrophobic pocket, which has been confirmed in the case of 4-4-20 by structural studies (*35*). Thus, the dynamics observed in the 3PEPS experiments are attributed to the protein and not to the solvent. In the case of Ab 4-4-20, this has been confirmed by MD simulations (*34, 36*). In addition, others have interpreted the spectroscopic and/or dynamic behavior of chromophores buried within protein in terms of protein motions (*49–53*).

The 3PEPS experiments reveal the amplitude and time scale of the motions that are displaced by the absorption-dependent change in electronic structure of the bound Fl. All six complexes show motions on three distinct time scales; fast (femtosecond), intermediate (picosecond), and slow (nanosecond and longer). To gauge the extent of diversity observed in the six Ab, it is instructive to compare the data to that obtained from other 3PEPS studies. Previous studies of protein−dye complexes found picosecond time scale motions that are similar to those found in Ab 4-4-20, 34F10, and 56G2. For example, a 7 ps decay was observed for eosin bound to lysozyme (*54*), and a 2 ps decay was observed for the chromophoric antigen 8-methoxypyrene-1,3,6,trisulfonic acid bound to an Ab (*43*). In contrast, the faster 0.6 to 0.8 ps motions found for Ab 18B7, 4D4, and 1F10 have only been observed for dyes in small molecule solvents (*29, 55*). Thus, the ∼10-fold variation in τ_k appears to reflect significant differences in the diffusive motions of the combining site among the six Ab. A relatively large variation in static inhomogeneity was found with the different Fl Ab in this study, ranging from 136 to 301 cm^{-1}. In comparison, values of static inhomogeneity for the dye IR144 were found to vary from zero in polar solvents (*56*) to 500 cm^{-1} in PMMA glass (*57*). Glasses are known to be very heterogeneous and static; therefore, the value of 500 cm^{-1} may represent an upper limit for experimentally observable static inhomogeneity. This suggests that the ∼200 cm^{-1} variance in static inhomogeneity for the anti-Fl Ab is large, and furthermore, it suggests that Ab 1F10, with a static inhomogeneity of 301 cm^{-1}, is remarkably heterogeneous and plastic. It should be noted that for Ab 18B7, 1F10, and 4D4, the experimental time window is limited by fast population decays of 8, 24, and 34 ps, respectively; therefore, decays on a longer time scale may appear static and thus contribute to static inhomogeneity. However, if this were the case, it would imply the existence of even greater differences in the diffusive motions of the combining sites. Regardless, the overall diversity in dynamics among the six Ab appears to be significant, and this suggests that the immune system has the potential to employ different mechanisms of molecular recognition to bind a single Ag.

Protein Dynamics and the Energy Landscape of Ab−Antigen Complexes. Fl can serve as a probe of Ab-combining site dynamics because its electronic transition frequency is sensitive to its protein environment. Conformational disorder leads to a distribution in transition frequencies in the Ab-Fl complexes, as evident from their highly inhomogeneously broadened linear absorption spectra. As the protein fluctuates within and between states, the changing environment induces shifts in the Fl transition frequency. In a 3PEPS experiment, this leads to dephasing and to a decay in the 3PEPS signal. The energy gap correlation function, $M(t)$, obtained from 3PEPS experiments thus reports on the sampling of accessible conformational phase space of the combining site over time. The time constants of the decay components observed in $M(t)$ are related to the frequency of motions within or between discrete states of the protein, while the corresponding amplitudes report on the amount of phase space sampled by a particular decay component.

The observation of distinct time scales of motion in the Ab-Fl complexes is not consistent with a continuum of motions within the Ab, but rather is reminiscent of Frauenfelder's model of a hierarchical energy landscape wherein a protein exists in a limited number of conformations, each consisting of a large number of conformational substates (*58, 59*). The three distinct time scales of motion observed in the Ab-

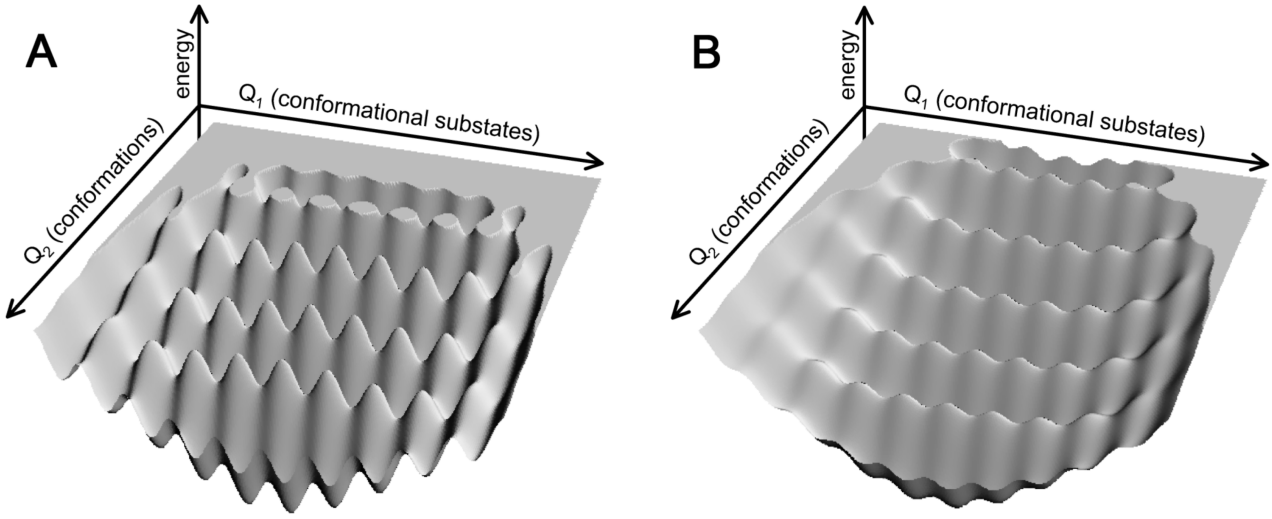

FIGURE 6: Representation of Ab energy landscapes (A) for 4-4-20, the most rigid Ab in this study, and (B) for 1F10, the most flexible Ab in this study. Conformational substates are separated by higher barriers in 4-4-20 than 1F10 (Q_1 dimension), and 4-4-20 samples have less phase space through conformational dynamics (Q_2 dimension) than 1F10. The flexibilities of the other Ab characterized are intermediate between 4-4-20 and 1F10.

Fl complexes are thus interpreted as different ranks of protein fluctuations. Inertial motions within the single well of a conformational substate, which are essentially barrierless, give rise to the femtosecond time scale component; diffusive motions between different conformational substates separated by relatively small barriers give rise to the picosecond time scale component; and conformational changes that must overcome relatively large barriers give rise to motion on longer (static) time scales (*49, 60*). Accordingly, in $M(t)$ the frequency and damping of the femtosecond Brownian oscillator term describe the time scale of the inertial motions, and the time constant associated with the picosecond Kubo term is related to the average barrier height between conformational substates. Interestingly, one of the most significant differences observed among the Ab is in τ_k, the time constant of the diffusive motions, which varies by almost an order of magnitude and corresponds to approximate average activation barriers of 0.8 to 2.1 kcal/mol (*61*). The largest barriers between conformational substates are found for Ab 4-4-20, and thus, we conclude that the potential energy surface of this Ab, at least the part probed by Fl excitation, is the most rugged. The barriers are smaller in 34F10 and 56G2, being approximately 1.6 kcal/mol, and the lowest in 18B7, 4D4 and 1F10, with average barriers of only 0.8 to 1.0 kcal/mol. This leads to a rather different picture of thermal motion in the different Ab: barriers in 4-4-20 are significantly greater than k_bT, while those in 1F10 are on the order of k_bT.

No significant differences are found in the amplitudes of the inertial motion, λ_{BO}; however larger differences are found in the amplitudes of the diffusive motion, λ_K, and static inhomogeneity, Δ_{inh} (Table 3). Each of these amplitudes (λ_{BO}, λ_K, and Δ_{inh}) represents the contribution of the corresponding protein motion to the relaxation of the chromophore's $S_1 - S_0$ energy gap after photoexcitation and thus the amount of phase space sampled by the motion (see above). When considering the normalized contribution of each time scale of motion (Table 4), it is apparent that the reorganization of the 4-4-20 and 56G2 combining sites are dominated by inertial motions (~70% amplitude) with less and relatively similar contributions from diffusive motions and conformational dynamics (~15%). In comparison, reorganization of 1F10 results from a roughly equal contribution of inertial motion and conformational dynamics (40−44%) with a lesser contribution from diffusive motions (15%). The Ab with the greatest relative contributions of diffusive motions are 34F10 and 4D4 (21−25%). These results indicate that the Ab combining site motions result from rather different superpositions of the three tiers of conformational fluctuations. In Ab 4-4-20 and 56G2, the accessible phase space is sampled predominantly by high-frequency, localized motions on the subpicosecond time scale. In the other Ab, increasingly more of the accessible phase space is sampled through lower frequency motions on the picosecond or longer time scale, which correspond to larger scale diffusive motions or conformational dynamics.

It is instructive to consider the data in terms of protein flexibility. As with any material, protein flexibility involves both elasticity and plasticity. Elastic motions correspond to motion within a well, i.e., reversible fluctuations within a conformational substate. Fluctuations that involve passage over a barrier to a different substate contribute to protein plasticity. Accordingly, the Brownian oscillator term in $\rho_{Ab}(\omega)$, describing motion within a substate well, quantifies elastic contributions to flexibility, while the Kubo term and static inhomogeneity quantify plasticity. In terms of both elasticity and plasticity, 4-4-20 is the most rigid Ab. It possesses the greatest relative contribution of high frequency elastic motion and the highest barriers separating the conformational substates explored on the picosecond time scale, and it is the least conformationally diverse of the Ab (Figure 6A). In contrast, Ab 1F10 is the most flexible, with the smallest contribution of high frequency elastic motion, conformational substates separated by the lowest barriers, and the greatest conformational diversity (Figure 6B). The other Ab also show a clear correlation between the relative contribution of elastic motions, the height of the barrier separating conformational substates, and conformational diversity. Thus, the trends in elasticity and plasticity together generate a rather consistent picture of the relative flexibility of the different Ab, with 4-4-20 being the most rigid and 1F10 the most flexible.

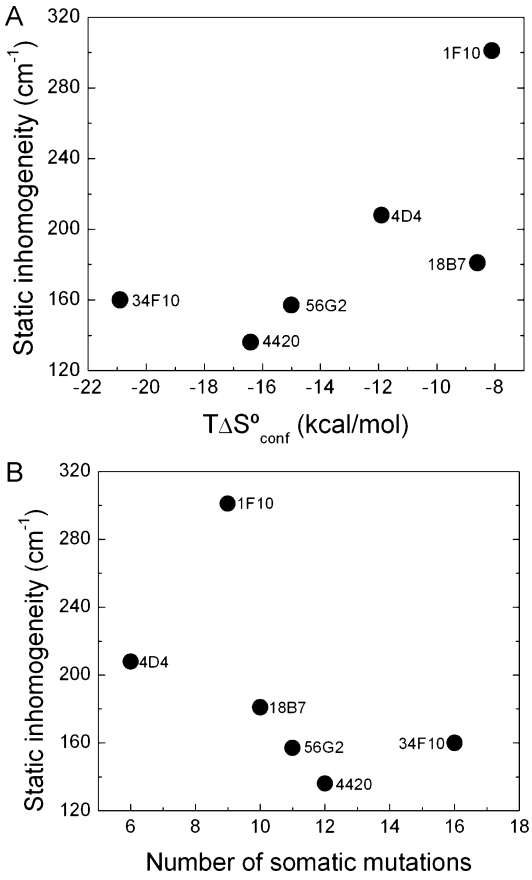

FIGURE 7: Correlations between static inhomogeneity and (A) conformational entropy ($T = 298$ K) or (B) the number of somatic mutations acquired during affinity maturation.

Correlations between Protein Dynamics and Thermodynamics, Germline Gene Use, and Somatic Mutation. The observed trends in flexibility are at least roughly correlated with thermodynamic behavior (Figure 7A). The Ab that appear most rigid show the most negative binding entropy, and the Ab that are most flexible show the most favorable binding entropy. While a mechanistic interpretation of this data requires comparison to the flexibility of the free Ab and unbound Fl, the data implies that the observed differences in binding entropy originate from the loss of conformational entropy upon complex formation. Regardless of the mechanistic interpretation, the data suggest that dynamics contribute to antigen recognition and that the differences in dynamics are reflected in the flexibility of the Ab−antigen complexes.

A correlation is also apparent between Ab dynamics, germline gene use, and the extent of affinity maturation (Figure 7B). The more somatically mutated Ab, on average, show a lower static inhomogeneity. In addition, when considering all of the Ab, more than half of the somatic mutations appear to occur in framework regions, away from the CDR loops that are expected to contact Fl. As already suggested for Ab 4-4-20 (*33, 34*), these data strongly suggest that at least some of the somatic mutations were selected on the basis of secondary interactions that act from a distance to localize the combing site to a specific conformation, presumably one appropriate for antigen binding.

The Ab that evolved from common V_H germline genes, Ab 34F10 and 56G2, and Ab 18B7 and 4D4, generally show similar dynamics, suggesting that these V_H make important contributions to combining site dynamics. However, λ_k, the contribution of diffusive motions to the reorganization energy, is different in Ab 34F10 and 56G2. This difference must result from the different CDR3 sequences installed during recombination, the different somatic mutations, or from the different V_L chains employed. Interestingly, recombination resulted in two sequential Pro residues in the 34F10 V_H CDR3, while it resulted in two Gly residues at an analogous position in 56G2, and it seems likely that these sequence differences contribute to the differences in dynamics. Two identical somatic mutations, K52bR and S67N, occurred in both 34F10 and 56G2, and Gly16 was mutated to either a Asn (in 34F10) or an Asp (in 56G2), suggesting that they are important for Fl recognition. Otherwise, the somatic mutations acquired in the common V_H chains are different, and thus, they too may contribute to the different dynamics in 34F10 and 56G2.

The data clearly demonstrate that the immune system is capable of generating Ab with a wide range of dynamics and thus complement the vast amount of sequence diversity data already available. Moreover, the at least approximate correlations observed between dynamics, thermodynamics, germline gene use, and somatic mutation suggests that the observed diversity of dynamics is biologically relevant. Dynamic diversity may have been a strong selection pressure that helped shape the germline gene repertoire to ensure that rigid Ab, which perhaps function via lock-and-key-like mechanisms, are available to rapidly respond to commonly encountered antigens but that more flexible Ab are also available, which perhaps function via induced fit or conformational selection and thus are more likely to bind new or rare antigens. When necessary, somatic mutations may rigidify the flexible Ab, thus making them more specific. This is an especially interesting hypothesis considering the need to convert polyspecific germline Ab that recognize a broad range of target antigen with an induced fit or conformational selection mechanism into more specific Ab that recognize only their target with a lock-and-key mechanism (*23, 62*), as has already been suggested for Ab 4-4-20 (*33, 34*). This hypothesis may be further tested by characterizing the germline Ab themselves and by using NMR spectroscopy, which can characterize dynamics on longer time scales as well as in the free Ab. Such experiments are underway and promise to help understand the immune system and elucidate the mechanisms underlying molecular recognition in general.

ACKNOWLEDGMENT

We thank Professors Shaul Mukamel (UC Irvine) and Peter Wolynes (UC San Diego) for helpful comments.

SUPPORTING INFORMATION AVAILABLE

Details of germline gene assignment, thermodynamic analysis, and statistical analysis. This material is available free of charge via the Internet at http://pubs.acs.org.

REFERENCES

1. Landsteiner, K. (1962) *The Specificity of Serological Reactions*, Dover, New York.
2. Cunningham, A. J. (1976) *The Generation of Antibody Diversity: A New Look*, Academic Press, London.

3. Alt, F. W., Blackwell, K., and Yancopoulos, G. D. (1987) Development of the primary antibody repertoire. *Science 238*, 1079–1087.
4. Tonegawa, S. (1983) Somatic generation of antibody diversity. *Nature 302*, 575–581.
5. Steele, E. J. (1990) *Somatic Hypermutation in V-Regions*, CRC Press, Boca Raton, FL.
6. Berek, C., and Milstein, C. (1988) The dynamic nature of the antibody repertoire. *Immunol. Rev. 105*, 5–26.
7. Gao, J., Byun, K. L., and Kluger, R. (2004) Catalysis by enzyme conformational change. *Top. Curr. Chem. 238*, 113–136.
8. Agarwal, P. K. (2006) Enzymes: An integrated view of structure, dynamics and function. *Microbial Cell Fact. 5*, 2–13.
9. Eisenmesser, E. Z., Bosco, D. A., Akke, M., and Kern, D. (2002) Enzyme dynamics during catalysis. *Science 295*, 1520–1523.
10. Daniel, R. M., Dunn, R. V., Finney, J. L., and Smith, J. C. (2003) The role of dynamics in enzyme activity. *Annu. Rev. Biophys. Biomol. Struct. 32*, 69–92.
11. Villa, J., and Warshel, A. (2001) Energetics and dynamics of enzymatic reactions. *J. Phys. Chem. B 105*, 7887–7907.
12. Wright, P. E., and Dyson, H. J. (1999) Intrinsically unstructured proteins: re-assessing the protein structure-function paradigm. *J. Mol. Biol. 293*, 321–331.
13. Kern, D., and Zuiderweg, E. R. P. (2003) The role of dynamics in allosteric regulation. *Curr. Opin. Struct. Biol. 13*, 748–757.
14. Jerne, N. K. (1955) The natural-selection theory of antibody formation. *Proc. Natl. Acad. Sci. U.S.A. 41*, 849–856.
15. Burnet, F. M. (1957) A modification of Jerne's theory of antibody production using the concept of clonal selection. *Aust. J. Sci. 20*, 67–69.
16. Breinl, F., and Haurowitz, F. (1930) Chemical examinations on the precipitate from haemoglobin and anti-haemoglobin serum and comments on the nature of antibodies. *Z. Physiol. Chem. 192*, 45–57.
17. Pauling, L. (1940) A theory of the structure and process of formation of antibodies. *J. Am. Chem. Soc. 62*, 2643–2657.
18. Silverstein, A. M. (2003) Splitting the difference: the germline-somatic mutation debate on generating antibody diversity. *Nat. Immunol. 4*, 829–833.
19. Manivel, V., Sahoo, N. C., Salunke, D. M., and Rao, K. V. S. (2000) Maturation of an antibody response is governed by modulations in flexibility of the antigen-combining site. *Immnunity 13*, 611–620.
20. Foote, J., and Milstein, C. (1994) Conformational isomerism and the diversity of antibodies. *Proc. Natl. Acad. Sci. U.S.A. 91*, 10370–10374.
21. Berzofsky, J. A. (1985) Intrinsic and extrinsic factors in protein antigenic structure. *Science 229*, 932–940.
22. Rini, J. M., Schulze-Gahmen, U., and Wilson, I. A. (1992) Structural evidence for induced fit as a mechanism for antibody-antigen recognition. *Science 255*, 959–965.
23. Wedemayer, G. J., Patten, P. A., Wang, L. H., Schultz, P. G., and Stevens, R. C. (1997) Structural insights into the evolution of an antibody combining site. *Science 276*, 1665–1669.
24. Kondo, H., Shiroishi, M., Matsushima, M., Tsumoto, K., and Kumagai, I. (1999) Crystal structure of anti-hen egg white lysozyme antibody (HyHEL-10) Fv-antigen complex: Local structural changes in the protein antigen and water-mediated interactions of Fv-antigen and light chain-heavy chain interfaces. *J. Biol. Chem. 274*, 27623–27631.
25. Nair, D. T., Singh, K., Siddiqui, Z., Nayak, B. P., Rao, K. V. S., and Salunke, D. M. (2002) Epitope recognition by diverse antibodies suggests conformational convergence in an antibody response. *J. Immunol. 168*, 2371–2382.
26. Li, Y. L., Li, H. M., Yang, F., Smith-Gill, S. J., and Mariuzza, R. A. (2003) X-ray snapshots of the maturation of an antibody response to a protein antigen. *Nat. Struct. Biol. 10*, 482–488.
27. James, L. C., Roversi, P., and Tawfik, D. S. (2003) Antibody multispecificity mediated by conformational diversity. *Science 299*, 1362–1367.
28. Cho, M., Yu, J.-Y., Joo, T., Nagasawa, Y., Passino, S. A., and Fleming, G. R. (1996) The integrated photon echo and solvation dynamics. *J. Phys. Chem. 100*, 11944–11953.
29. de Boeij, W. P., Pshenichnikov, M. S., and Wiersma, D. A. (1996) System-bath correlation function probed by conventional and time-grated stimulated photon echo. *J. Phys. Chem. 100*, 11806–11823.
30. Fleming, G. R., and Cho, M. H. (1996) Chromophore-solvent dynamics. *Annu. Rev. Phys. Chem. 47*, 109–134.
31. Mukamel, S. (1995) *Principles of Nonlinear Optical Spectroscopy*, Oxford University Press, New York.
32. Jimenez, R., Salazar, G., Baldridge, K. K., and Romesberg, F. E. (2003) Flexibility and molecular recognition in the immune system. *Proc. Natl. Acad. Sci. USA 100*, 92–97.
33. Jimenez, R., Salazar, G., Yin, J., Joo, T., and Romesberg, F. E. (2004) Protein dynamics and the immunological evolution of molecular recognition. *Proc. Natl. Acad. Sci. USA 101*, 3803–3808.
34. Zimmermann, J., Oakman, E. L., Thorpe, I. F., Shi, X. H., Abbyad, P., Brooks, C. L., Boxer, S. G., and Romesberg, F. E. (2006) Antibody evolution constrains conformational heterogeneity by tailoring protein dynamics. *Proc. Natl. Acad. Sci. U.S.A. 103*, 13722–13727.
35. Whitlow, M., Howard, A. J., Wood, J. F., Voss, E. W., Jr., and Hardman, K. D. (1995) 1.85 Å structure of anti-fluorescein 4-4-20 Fab. *Protein Eng. 8*, 749–761.
36. Thorpe, I., and Brooks, C. (2007) Molecular evolution of affinity and flexibility in the immune system. *Proc. Natl. Acad. Sci. U.S.A. 104*, 8821–8826.
37. Sastry, L., Alting-Mees, M., Huse, W. D., Short, J. M., Sorge, J. A., Hay, B. N., Janda, K. D., Benkovic, S. J., and Lerner, R. A. (1989) Cloning of the immunological repertoire in *Escherichia coli* for generation of monoclonal catalytic antibodies: construction of a heavy chain variable region-specific cDNA library. *Proc. Natl. Acad. Sci. U.S.A. 86*, 5728–5732.
38. Ulrich, H. D., Patten, P. A., Yang, P. L., Romesberg, F. E., and Schultz, P. G. (1995) Expression studies of catalytic antibodies. *Proc. Natl. Acad. Sci. U.S.A. 92*, 11907–11911.
39. Lefranc, M.-P., G., V., Kaas, Q., Duprat, E., Jabado-Michaloud, J., Scaviner, D., Ginestoux, C., Clément, O., Chaume, D., and Lefranc, G. (2005) MGT, the international ImMunoGeneTics information system. *Nucleic Acids Res. 33*, D593–D597.
40. Murphy, K. P., Freire, E., and Paterson, Y. (1995) Configurational effects in antibody-antigen interactions studies by microcalorimetry. *Proteins: Struct., Funct., Genet. 21*, 83–90.
41. Murphy, K. P., Privalov, P. L., and Gill, S. J. (1990) Common features of protein unfolding and dissolution of hydrophobic compounds. *Science 247*, 559–561.
42. Murphy, K. P., Xie, D., Thompson, K. S., Amzel, L. M., and Freire, E. (1994) Entropy in biological binding processes: Estimation of translational entropy loss. *Proteins 18*, 63–67.
43. Jimenez, R., Case, D. A., and Romesberg, F. E. (2002) Flexibility of an antibody binding site measured with photon echo spectroscopy. *J. Phys. Chem. B 106*, 1090–1103.
44. Kang, J. H., and Warren, A. S. (2007) Enthalpy-entropy compensation in the transition of a monospecific antibody towards antigen-binding promiscuity. *Mol. Immunol. 44*, 3623–3624.
45. Dunitz, J. D. (1995) Win some, lose some: Enthalpy-entropy compensation in weak intermolecular interactions. *Chem. Biol. 2*, 709–712.
46. Spolar, R. S., Livingstone, J. R., and Record, M. T. (1992) Use of liquid-hydrocarbon and amide transfer data to estimate contributions to thermodynamic functions of protein folding from the removal of nonpolar and polar surface from water. *Biochemistry 31*, 3947–3955.
47. Xu, Q.-H., Scholes, G. D., Yang, M., and Fleming, G. R. (1999) Probing solvation and reaction coordinates of ultrafast photoinduced electron-transfer reactions using nonlinear spectroscopies: rhodamine 6G in electron-donating solvents. *J. Phys. Chem. A 103*, 10348–10358.
48. Yang, M., Ohta, K., and Fleming, G. R. (1999) Three-pulse photon echoes for model reactive systems. *J. Chem. Phys. 110*, 10243–10252.
49. Homoelle, B. J., Edington, M. D., Diffey, W. M., and Beck, W. F. (1998) Stimulated photon-echo and transient-grating studies of protein-matrix solvation dynamics and interexciton-state radiationless decay in a phycocyanin and allophycocyanin. *J. Phys. Chem. B 102*, 3044–3052.
50. Yu, J.-Y., Nagasawa, Y., van Grondelle, R., and Fleming, G. R. (1997) Three pulse echo peak shift measurements on the B820 subunit of LH1 of *Rhodospirillum rubrum*. *Chem. Phys. Lett. 280*, 404–410.
51. Changenet-Barret, P., Choma, C. T., Gooding, E. F., DeGrado, W. F., and Hochstrasser, R. M. (2000) Ultrafast dielectric response of proteins from dynamic Stokes shifting of coumarin in calmodulin. *J. Phys. Chem. B 104*, 9322–9329.
52. Cohen, B. E., McAnaney, T. B., Park, E. S., Jan, Y. N., Boxer, S. G., and Jan, L. Y. (2002) Probing protein electrostatics with a synthetic fluorescent amino acid. *Science 296*, 1700–1703.

53. Kennis, J. T. M., Larsen, D. S., Ohta, K., Facciotti, M. T., Glaeser, R. M., and Fleming, G. R. (2002) Ultrafast protein dynamics of bacteriorhodopsin probed by photon echo and transient absorption spectroscopy. *J. Phys. Chem. B 106*, 6067–6080.
54. Jordanides, X. J., Lang, M. J., Song, X., and Fleming, G. R. (1999) Solvation dynamics in protein environments studied by photon echo spectroscopy. *J. Phys. Chem. B 103*, 7995–8005.
55. Larsen, D. S., Ohta, K., and Fleming, G. R. (1999) Three pulse photon echo studies of nondipolar solvation: comparison with a viscoelastic model. *J. Chem. Phys. 111*, 8970–8979.
56. Passino, S. A., Nagasawa, Y., Joo, T., and Fleming, G. R. (1997) Three-pulse echo peak shift studies of polar solvation dynamics. *J. Phys. Chem. A 101*, 725–731.
57. Nagasawa, Y., Passino, S. A., Joo, T., and Fleming, G. R. (1997) Temperature dependence of optical dephasing in an organic polymer glass (PMMA) from 300 to 30 K. *J. Chem. Phys. 106*, 4840–4852.
58. Frauenfelder, H., Parak, F. G., and Young, R. D. (1988) Conformational substates in proteins. *Annu. Rev. Biophys. Biophys. Chem. 17*, 451–479.
59. Frauenfelder, H., Sligar, S. G., and Wolynes, P. G. (1991) The energy landscape and motions of proteins. *Science 254*, 1598–1603.
60. Parak, F. G. (2003) Proteins in action: The physics of structural fluctuations and conformational changes. *Curr. Op. Struct. Biol. 13*, 552–557.
61. Eyring, H. (1935) The activated complex in chemical reactions. *J. Chem. Phys. 3*, 107–115.
62. Sundberg, E. J., and Mariuzza, R. A. (2003) Molecular recognition in antibody-antigen complexes. *Adv. Protein Chem. 61*, 119–160.

BI800374Q